JOURNAL OF THERMOPHYSICS AND HEAT TRANSFER
Vol. 25, No. 1, January–March 2011

Dissociation Modeling in Hypersonic Flows Using State-to-State Kinetics

Eswar Josyula*
U.S. Air Force Research Laboratory, Wright-Patterson Air Force Base, Ohio 45433
William F. Bailey†
Air Force Institute of Technology, Wright-Patterson Air Force Base, Ohio 45433
and
Casimir J. Suchyta III‡
U.S. Air Force Research Laboratory, Wright-Patterson Air Force Base, Ohio 45433

DOI: 10.2514/1.49903

Numerical simulations are presented of steady-state hypersonic blunt-body nitrogen flow for conditions under which there is considerable thermal dissociation. The internal energy relaxation processes of vibrational energy transfer and dissociation were treated using state-to-state kinetics of diatomic nitrogen. To gain understanding of the role of vibrational–translational rates on dissociation, the vibrational–translational rates were implemented in a ladder-climbing model, and the effect of vibrational bias on dissociation was investigated. For temperatures up to 25,000 K, a simplified depletion model with two different sets of vibrational–translational rates established the sensitivity of depletion to the relative magnitude of vibrational–translational and dissociation rates for dissociation in nitrogen. State-specific vibrational–translational and dissociation rates were incorporated into a solution of the master kinetic equations and coupled to the fluid dynamic equations to describe the thermochemical nonequilibrium phenomenon in high-temperature hypersonic flowfields. The flowfield consists of a Mach 19.83 nitrogen flow past a hemisphere cylinder with a radius of 0.1524 m. The full state-specific dissociation model, consisting of 48 quantum levels in the vibrational manifold, was coupled to the fluid dynamic equations. For temperatures in the shock layer ranging from 9000 to 21,000 K, the dissociation primarily takes place from the lower energy levels.

Nomenclature

D	=	dissociation energy
e	=	total energy per unit mass
ϵ_v	=	quantum level energy
k	=	Boltzmann constant
k_{v_D}	=	state-specific dissociation rate coefficient
$\bar{k}_{v_D}$	=	state-specific recombination rate coefficient
M	=	Mach number
$\mathcal{M}$	=	molecular weight, kg/mole
N	=	number density
N_{tot}	=	total molecular number density
n_0	=	total number of vibrational quantum levels
p	=	pressure, N/m^2
R	=	gas constant
T	=	equilibrium transrotational temperature
T_v	=	first-level (1,0) vibrational temperature
$\mathbf{u}$	=	velocity vector
v, v'	=	vibrational quantum numbers
ρ	=	total mass density
ρ_v	=	state density in vibrational quantum level v

Presented as Paper 2009-1579 at the 47th AIAA Aerospace Sciences Meeting, Orlando, FL, 5–8 January 2009; received 16 March 2010; revision received 11 October 2010; accepted for publication 12 October 2010.

*Senior Research Aerospace Engineer, Air Vehicles Directorate, 2210 Eighth Street. Associate Fellow AIAA.
†Associate Professor of Physics, Department of Engineering Physics, 2950 Hobson Way.
‡Senior Researcher, Ohio Aerospace Institute, 2210 Eighth Street.

I. Introduction

HIGH-VELOCITY flows in flight vehicles create many situations where rapid changes occur in flow variables, such as density, specific energy, and temperatures. The relatively long equilibration time of the internal energy modes compared with the characteristic flow time causes nonequilibrium in the rotational, electronic, and chemical energy modes. The present study is about the chemical energy modes, specifically the modeling of dissociation of nitrogen in high speed flow past a blunt body. It is well known that at high temperatures, the reaction paths and the reaction rates have many uncertainties, even for air chemistry. Although extensive shock tube data exist, they exhibit considerable scatter and disagreements. Studies have shown that even a practical quantity like the shock standoff distance can vary as much as 18%, due to the uncertainty in vibration–dissociation relaxation rates [1]. More recently in a study with chemical reaction rates [2], the wall heat flux variation predicted by using different state-to-state kinetic models was in the range of 12–16% and between different one temperature models as high as 11%. The present study is an attempt to address some of the uncertainties in the underlying energy-transfer mechanisms in the full state-to-state modeling of dissociation in a hypersonic flow past a blunt body for conditions encountered in a reentry flow.

It has long been recognized that to study chemical kinetics in the thermal nonequilibrium state, it is necessary to consistently examine the vibrational relaxation process in a reacting gas. The state-to-state kinetic models of vibrational relaxation give the desired mass concentrations and mean vibrational energy of molecules as a function of time for chemically reacting gas. The primary assumption of these models is that the characteristic time of vibrational relaxation is much greater than the translational and rotational relaxation, but is comparable with the characteristic time of chemical reaction. In the upper levels of the vibrational manifold, the vibrational–translational (V-T) processes dominate the energy transfer. The reactive process of dissociation has an activation energy typically over an order of magnitude greater than the energy associated with the V-T exchange. The nonreactive and reactive processes have contrasting effects on the state of nonequilibrium. Nonreactive kinetic processes tend to

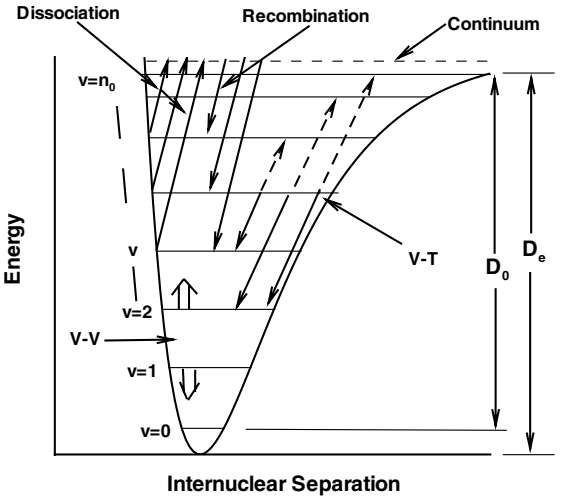

Fig. 1 Schematic showing various rates processes in the vibrational states.

bring about an equilibrium distribution in the vibrational manifold, whereas the dissociation process perturbs it [3]. Figure 1 shows a schematic of various energy-transfer mechanisms used to describe thermochemical nonequilibrium.

The semiclassical approach to diatom–diatom and atom–diatom collision problem gives a fast and reliable calculation of a large number of rate constants if the potential energy surface is provided. Using this calculation approach, Billing [4–6] advanced the theory to calculate the state-to-state rates of single quantum vibrational–vibrational (V-V) and V-T transfers for nitrogen collisions. Capitelli et al. [7] and Billing and Fisher [8] considered single quantum transitions and empirically determined the V-T rates from semiclassical calculations verified by experiments. The forced harmonic oscillator (FHO) theory, an approximation of Billing's [4–6] method, was adopted by Macheret and Adamovich [9] for developing a theory of dissociation of diatomic molecules based on the anharmonicity-corrected and energy-symmetrized FHO quantum scaling [10] in conjunction with free-rotation or impulsive energy-transfer models. The model predicts state-specific dissociation rates for N_2–N_2 collisions by accounting for molecular rotation and three-dimensional collisions and is computationally tractable without any adjustable parameters. More recently, a first-principles approach was attempted [11] for the N–N_2 collisions for calculating state-to-state dissociation rate constants with the ultimate goal of assessing heating rates on hypersonic vehicles.

Other recent studies address some of the deficiencies in the current semi-empirical approaches and suggest improvements. For example, da Silva et al. [12] constructed a database of kinetic rates for nitrogen for high-temperature (up to 100,000 K) nonequilibrium dissociation processes for use in flowfield simulations of vehicles at atmospheric entries. This modification to the FHO model consists of energies of 59 bound vibrational levels of the nitrogen molecule, an increase from the earlier work (see, for example, [9]) of 48 vibrational quantum levels for dissociation. The increase was determined through the reconstruction of the ground-state potential curve according to the Rydberg–Klein–Rees method, relying on the latest spectroscopic data. The work of Shui et al. [13] demonstrates the contribution of the $N_2A^3\sum$ metastable electronic state, which were used in modeling of the nonequilibrium distributions in hypersonic flows past solid bodies by Armenise et al. [14] and in a nozzle flow by Colonna and Capitelli [15]. A reduced-order nitrogen dissociation model from state kinetic rates was presented by Colonna et al. [16]. Attempts at applying the kinetic rates are presented by Armenise et al. [17], who used the quasi-classical molecular dynamic calculations of vibrationally and rotationally state selected dissociation cross sections for nitrogen atom–molecule collisions and used them to evaluate dissociation-recombination kinetics in hypersonic boundary-layer flows. Recently, the quasi-classical trajectory calculations by Esposito and Capitelli [18] reported complete set of V-T rates in the temperature range of 500–4000 K for the $N_2(v) + N \rightarrow N_2(v') + N$. The work by Armenise et al. [19,20] modeled the kinetic processes and heterogeneous surface processes in the boundary layer of reentry vehicles and demonstrated the highly nonequilibrium vibrational distributions and the non-Arrhenius behavior of dissociation constants. Armenise et al. [19] demonstrated the recombination assisted dissociation process resulting in non-Arrhenius behavior of the dissociation constant affecting the surface heat transfer. However, for the present study of a shock wave flow, the effect of recombination is expected to be small, and as a first step in the numerical modeling of the state-to-state process of the dissociation process, the recombination process is neglected.

The kinetics of thermal dissociation has long been a topic of theoretical research, due to the difficulty of reconciling the measured rates within the framework of the flowfield (see, for example, [21]). In a ladder-climbing model, vibrational excitation occurs from the ground state to higher energy states and, conversely, the deexcitation from the higher energy states to the lower energy states and finally back to the ground state, with the state-to-state transitions occurring in single- or multiple quantum jumps. The excitation and deexcitation phases proceed at different rates, with the result that the vibrational manifold begins to build up its internal energy. Dissociation takes place when the internal energy exceeds the dissociation energy D_0 (Fig. 1). When the rate of dissociation is greater than the rate at which the internal energy builds up in the vibrational manifold, vibrational population gets depleted. Although depletion originates in the dissociating vibrational state, in order to replenish the quanta in this energy state the depletion is coupled to other energy states as well. Dissociation can occur from any or all of the vibrational levels. However, for certain temperature ranges there is a distinct vibrational bias to dissociation; a strong bias implies dissociation takes place from the last level or any of the upper levels and a weak bias indicates that dissociation is distributed over the entire vibrational manifold. The present work shows the development of weak and strong-bias models that allow us to examine bias for different V-T rates and temperature conditions.

The motivation for the current study is the inadequacy of the current modeling techniques used in the prediction of macroscopic flow variables in hypersonic aerothermodynamics. Currently, the popular modeling techniques of modeling vibrational relaxation using the Landau and Teller [28] approach and modeling dissociation using the Park [22] two-temperature model are limited in the range of applicability in hypersonic flow applications. Modeling the nonequilibrium relaxation processes using the physics-based state-to-state kinetics is a major advancement from current modeling techniques with the promise of greater accuracy, reliability, and wider range of applicability in the hypersonic regime. However, these modeling techniques rely on the accuracy of the state kinetic rates, which exist for just a few species in the multicomponent high-temperature gaseous air mixture. The ability to couple state kinetic rates with fluid dynamic equations to simulate high-Mach-number flows for blunt-body flows is a considerable challenge, due to the large system of partial differential equations to solve and the stiffness associated with the source terms. The coupling of existing state kinetic rates for vibration and dissociation with the fluid dynamic equations to simulate a Mach 19 flow past a blunt body is performed for the first time in the present study. The objective is to compare the flowfields with different modeling techniques, to assess the sensitivity to rate variations, and to understand the nonequilibrium flow physics with different relaxation mechanisms. The long-term goal is to have a proper understanding of the nonequilibrium physics for developing reduced-order models for hypersonic real-gas applications.

The objective of this investigation was to use a self-consistent set of state-specific kinetic rates for dissociation and vibrational energy transfer to examine the interplay of vibrational bias and depletion on shock structure and standoff distance. Two sets of transfer rates are sampled to focus on depletion at high temperatures. In both sets the transfer is limited to single quantum transitions and V-V exchanges are excluded. Given our objective and recognizing the uncertainty in the scaling of multiple quantum rates, the neglect of multiple

quantum V-T is justified. At the elevated temperature considered, the single quantum V-T transfer rate becomes gas kinetic, suggesting that V-V exchanges would have minor effects on flow variables. The contribution of electronically excited states to the vibrational transfer and dissociation reaction is also excluded on the basis that direct impact excitation is improbable, even at these high temperatures, and vibration-to-electronic (V-E) transfer from the ground state will still be limited by the V-T exchanges in the ground electronic state, creating a rate-limiting bottleneck. Rates associated with V-E transfer and V-T, V-V, and dissociation coefficients in the excited electronic states are uncertain. Therefore, in order to maintain a focus on the stated objective, excited electronic states have been omitted from consideration. To bound the influence of the endothermic nature of the dissociation reaction on the macroscopic characteristics of the flow, recombination has been neglected. By considering the two cases of dissociation (no recombination) and the net dissociation of zero (dissociation and recombination in balance), the bound is achieved.

As a first step toward coupling the full state kinetic dissociation rates to the flow equations and assessing the effect of detailed kinetics on the flow, the recombination process has been neglected in the present study. Similarly, the role of excited electronic states, multiple quantum jumps and the V-V energy transfers are neglected in the present study for two reasons: 1) lack of reliable transition rates and 2) the additional complexity in coupling these rates processes to the system of equations. The present paper presents high-Mach-number flow simulations with dissociation modeled by 1) global non-equilibrium dissociation rate and 2) state-specific dissociation rate. To gain understanding of the competing effects of V-T and dissociation rates a simplified depletion model was used for defining a nonequilibrium global dissociation rate. The paper presents hypersonic flowfield simulations of a Mach 19.83 nitrogen flow past a hemisphere cylinder using the full state-to-state kinetic dissociation model with 48 vibrational quantum states. The effect of thermo-chemical nonequilibrium kinetics on shock standoff distance, temperatures, mass concentrations, and nonequilibrium population densities is examined.

II. Analysis

The global fluid dynamic conservation equations in mass-averaged velocity form to simulate a blunt-body flow are presented in this section. The inviscid Euler equations were coupled to the master kinetic equations to describe a high-temperature hypersonic flow in thermochemical nonequilibrium. The nonequilibrium state is simulated for the V-T process and the dissociation process with state kinetic rates:

$$\frac{\partial}{\partial t}(\rho_v) + \nabla \cdot (\rho_v \mathbf{u}) = \dot{\omega}_v \qquad v = 0, 1, \ldots \tag{1}$$

$$\frac{\partial}{\partial t}(\rho_N) + \nabla \cdot (\rho_N \mathbf{u}) = 0 \tag{2}$$

$$\frac{\partial}{\partial t}(\rho \mathbf{u}) + \nabla \cdot (\rho \mathbf{u}\mathbf{u} - p\bar{\bar{\delta}}) = 0 \tag{3}$$

$$\frac{\partial}{\partial t}(\rho e) + \nabla \cdot [\rho(e + p/\rho)\mathbf{u}] = 0 \tag{4}$$

Equations (1–4) describe the conservation of mass, momentum and energy in the flowfields of interest. Equation (1) is discussed further in the following section. Equations (3) and (4) represent the conservation of total momentum and energy, respectively. A microscopic kinetic approach was taken by treating the molecule as anharmonic oscillator, calculating the mass density in quantum level v, ρ_v, using the master equation.

A. Master-Equation Approach to Modeling Dissociation

The conservation Eq. (1) is written for the mass density in quantum level v. The source term $\dot{\omega}_v$ derived from the vibrational master equations is made up of the relevant energy exchange processes consisting of the V-T and dissociation processes. The mass density of the molecular species is the sum of the corresponding state densities in the vibrational levels:

$$\rho = \sum_{v=0}^{n_0} \rho_v \tag{5}$$

The symbolic equations governing the V-T transitions responsible for populating or depopulating the vth vibrational level are

$$\mathrm{N}_2(v) + \mathrm{N}_2 \rightleftharpoons \mathrm{N}_2(v') + \mathrm{N}_2 \tag{6}$$

and the equations governing the dissociation process considering dissociation to take place from any vibrational level:

$$\mathrm{N}_2(v) + \mathrm{M} \rightleftharpoons 2\mathrm{N} + \mathrm{M} \tag{7}$$

The state-specific dissociation rate coefficients of N_2–N_2 and N_2–N collisions for this reaction were implemented via the master kinetic equations. The kinetics of the particle exchanges among the quantum states are simulated using the vibrational master equations, and the population distributions are calculated with [23]

$$\begin{aligned}\dot{\omega}_v = \frac{1}{\mathcal{M}} \Bigg\{ & \sum_{v'} [k_{\mathrm{VT}}(v' \to v)\rho_{v'}\rho - k_{\mathrm{VT}}(v \to v')\rho_v \rho] \\ & + [-k_{vD}(v \to \text{continuum})\rho_v \rho_{\mathrm{N}_2} \\ & - \bar{k}_{vD}(\text{continuum} \to v)\rho_N \rho_N] \Bigg\}\end{aligned} \tag{8}$$

In the present calculations, the exchanges are restricted to single quantum transitions as a first attempt to coupling state-specific dissociation rates to the fluid dynamic equations. The V-T process is associated with the rate coefficient k_{VT}, where the molecule loses or gains a vibrational quantum. The transfer rate from v' to v for colliding molecules is denoted by $k_{\mathrm{VT}}(v' \to v)$, and the inverse collision from $v \to v'$ is denoted by $k_{\mathrm{VT}}(v \to v')$. The dissociation rate coefficient k_{vD} and $\bar{k}_{vD}$ are the state-specific rate coefficients for N_2–N_2 and N_2–N collisions, respectively.

For coupling the nonequilibrium kinetics with the fluid dynamic equations, single quantum vibrational-transition rate coefficients for V-T process are taken from the work of Adamovich and Rich [10], and state-specific dissociation rate coefficients are taken form Macheret and Adamovich [9]. A second set of V-T rate coefficients calculated according to expressions proposed in [24] for V-T rate coefficients of Capitelli et al. [7] and Billing and Fisher [8] were used for the purpose of studying sensitivity to depletion; these expressions [24] of V-T rate coefficients were not used to couple to the fluid dynamic equations for the simulation of the flowfield. The vibrational energy of the diatomic molecules N_2, treated as anharmonic oscillators, is given in terms of the quantum level energies by

$$e_{\mathrm{vib}} = \sum_{v=1}^{n_0} \frac{\rho_v}{\rho} \epsilon_v \tag{9}$$

where the index v enumerates the vibrational quantum level. In this equation, ρ_v/ρ is the fractional population of the vth vibrational level, and ϵ_v is the quantum level energy given by the second-order approximating formula:

$$\frac{\epsilon_i}{hc} = \omega_e\left(i - \frac{1}{2}\right) - x_e\left(i - \frac{1}{2}\right)^2 \qquad i - 1, 2, \ldots \tag{10}$$

where h is Planck's constant, c is the speed of light, ϵ_1 denotes ground-state vibrational energy, ϵ_2 denotes first excited state, and so on. The spectroscopic constants are given by [9], $\omega_e = 2359.6\ \mathrm{cm}^{-1}$,

and $x_e = 6.1265 \times 10^{-3}$. When $n_0 = 47$, the value of energy exceeds the N_2 dissociation energy: 9.75353 eV.

B. Modeling of Nonequilibrium Dissociation Based on Depletion Model

Vibrational population depletion due to dissociation was modeled to account for the internal energy mode relaxation in dissociating flows. This model was developed by Josyula and Bailey [25,26] and Josyula et al. [27], where the V-T and V-V transition rates were considered to study the effect of dissociation from the last level on the population depletion in the vibrational states. To couple the depletion model to the flow equations, the vibrational energy conservation equation was solved in addition to the conservation of mass, momentum, and energy equations. The V-T coupling in the vibrational energy equation was modeled according to the Landau–Teller form [28], with the interspecies relaxation time computed using expressions developed by Millikan and White [29]. The nonequilibrium dissociation rate, however, considered the competing time scales of the state-to-state kinetics of vibration with dissociation, briefly described here.

C. Depletion Model

In their study of the kinetics of thermal dissociation, Osipov and Stupochenko [3] showed that the vibrational population distribution function is altered by the dissociation process. As equilibrium is approached, a quasi-steady-state is achieved, and the populations obtain a self-similar form. The dissociation losses from the vibrational manifold tend to reduce the vibrational populations below their equilibrium values, resulting in the lowering of the dissociation rate. At equilibrium, there is no net gain or loss due to dissociation and recombination; hence, there is no depletion of the population from the vibrational manifold. It is convenient to divide the vibrational relaxation in to two time regimes. Initially, over a time τ_{VT} a quasi-steady distribution is established. Over a much longer time τ_{diss}, this distribution approaches the equilibrium distribution, and the atoms and molecular species concentrations then ultimately satisfy the law of mass action. Here, we consider the evolution of the quasi-steady distribution as it evolves in time toward the equilibrium distribution. With $\tau_{\mathrm{VT}} < t \leq \tau_{\mathrm{diss}}$, two opposing factors characterize this state: V-T trying to establish equilibrium and dissociation disrupting and perturbing the distribution. To simplify the analysis in the present study, dissociation is restricted to the last discrete vibrational level.

This section presents the kinetic equations describing the dissociative-relaxation coupling, considering the balance equations for the numbers of particles in each vibrational level [3]:

$$\dot{\rho_v} = \sum_{v'} [k_{\mathrm{VT}}(v' \to v)\rho_{v'}\rho_{\mathrm{N}_2} - k_{\mathrm{VT}}(v \to v')\rho_v\rho_{\mathrm{N}_2}] + k_{rv}\rho_{\mathrm{N}}^2\rho_{\mathrm{N}_2} - k_{dv}\rho_v\rho_{\mathrm{N}_2} \qquad v = 0, 1, \ldots l \tag{11}$$

$$\frac{1}{2}\dot{\rho}_{\mathrm{N}} = \sum_{v=0}^{l} k_{dv}\rho_v\rho_{\mathrm{N}_2} - \sum_{v=0}^{l} k_{rv}\rho_{\mathrm{N}}^2\rho_{\mathrm{N}_2} \tag{12}$$

where ρ_v is the mass density in level v, $k_{v' \to v}$ and $k_{v \to v'}$ are the V-T rate coefficients for vibrational transitions to occur from $v' \to v$ and $v \to v'$, k_{dv} and k_{rv} are the rate constants for dissociation/recombination in transition from/to vibrational state v to/from continuum, ρ_{N} is the density of nitrogen atoms resulting from dissociation and ρ_{N_2} is the number of colliding molecules, and l is the last discrete vibrational level of the molecule. Note that

$$\sum_{v=0}^{l} \rho_v = \rho_{\mathrm{N}_2}$$

If we can define φ_v to give the deviation of the quasi-steady distribution from an equilibrium Boltzmann distribution, then the mass density in vibrational state v is

$$\rho_v(t) = \rho_v^{(0)}(1 + \varphi_v) \tag{13}$$

The deviation of the population of level v from equilibrium is given by φ_v, which relates ρ_v (the state mass density in level v) to $\rho_v^{(0)}$ (the state mass density in level v at equilibrium). It is seen that when $\varphi_v < 0$, the level population *decreases* relative to the equilibrium population. The deviation coefficient φ_v in the simplest case of single quantum energy transitions and dissociation *only* from the last discrete vibrational level is given by

$$\varphi_v = \frac{\dot{\mathrm{N}}_2}{\rho_{\mathrm{N}}\rho_{\mathrm{N}_2}} \sum_{i=1}^{v} \frac{1}{k_{i-1,i}\Gamma_{i-1}} \left(\sum_{j=0}^{i-1} \Gamma_j \right) + \varphi_0 \tag{14}$$

where $\dot{\mathrm{N}}_2$ is the global rate of the dissociation reaction. The unknown φ_0 term, which gives the deviation for the first discrete vibrational level, is determined from the normalization condition for Eq. (13) given by

$$\sum_{v=0}^{l} \rho_v^{(0)}\varphi_v = 0$$

From this condition, it follows that

$$-\varphi_0 = \frac{1}{\rho_{\mathrm{N}_2}} \sum_{v=1}^{l} \rho_v^{(0)}\tilde{\varphi}_v \tag{15}$$

where $\tilde{\varphi}_v = \varphi_v - \varphi_0$. The Γ_v term is given by

$$\Gamma_v = \frac{e^{\frac{-\epsilon_v}{kT}}}{\sum_{v=0}^{l} e^{\frac{-\epsilon_{v'}}{kT}}} \tag{16}$$

See [25,30] for more detailed treatment of the depletion model. To assess the sensitivity of depletion to different V-T rates, depletion factors φ_v are presented in Eq. (13) for two sets of V-T rate coefficients for a wide range of temperatures.

D. Weak- and Strong-Bias Model Development

As mentioned earlier, dissociation can occur primarily from the higher energy states, herein termed as the strong-bias model, or from the lower energy states, termed as the weak-bias model. The two bounds of strong-bias and weak-bias models were developed considering the energy in the vibrational quantum states of the dissociating diatomic molecule to help identify the primary quantum levels contributing to dissociation across a wide temperature range. Dissociation in the strong-bias model is assumed to take place only from the last bound state, whereas for the weak-bias model *all* quantum states contribute. The dissociation rate of the strong-bias model can be written as

$$n_{v^*}k_{v^* \to \mathrm{continuum}} \tag{17}$$

where n_{v^*} is the vibrational population in the last state and $k_{v^* \to \mathrm{continuum}}$ is the dissociation rate from the last vibrational state.

The weak-bias model, in contrast to the previous model, assumes dissociation to proceed from all the states, viz., $n_0k_{0 \to \mathrm{continuum}}$, $n_1k_{1 \to \mathrm{continuum}}$, $n_2k_{2 \to \mathrm{continuum}}$, and so on, to $n_{v^*}k_{v^* \to \mathrm{continuum}}$.

To facilitate a comparison of the global rate of dissociation under different conditions of vibrational bias, it is useful to define an effective dissociation rate $k_{d_{\mathrm{eff}}}[T, T_v]$, where

$$k_{d_{\mathrm{eff}}}[T, T_v]N_{\mathrm{tot}} \equiv \sum_{v=0}^{v^*} k_{d_v}n_v \tag{18}$$

and k_{d_v} is the dissociation coefficient from vibrational state v and is assumed to be a function of T only. By expressing the functional dependence of the population in each vibrational state in terms of a vibrational temperature,

$$n_v = \frac{N_{\text{tot}} \exp\left(\frac{-\epsilon_v}{kT_v}\right)}{Z_{\text{vib}}} \tag{19}$$

where Z_{vib} is the vibrational partition function, ϵ_v is the vibrational energy in the quantum level v, k is the Boltzmann constant, N_{tot} is the total number density, and T_v is the vibrational temperature. One can express the $k_{d_{\text{eff}}}[T, T_v]$ for the strong-bias and weak-bias models in terms of the equilibrium coefficient $k_d[T]$. In equilibrium,

$$k_{d_{\text{eq}}}[T] = \sum_{v=0}^{v^*} k_{d_v} \frac{n_{v_{\text{eq}}}}{N_{\text{tot}}} = \sum_{v=0}^{v^*} k_{d_v} \frac{\exp[-\epsilon_v/kT]}{Z_{\text{vib}}[T]} \tag{20}$$

For the strong-bias model,

$$\begin{aligned} k_{d_{\text{eff}}}[T, T_v] &= k_{d_{v^*}} \frac{n_{v^*}}{N_{\text{tot}}} = k_{d_{\text{eq}}}[T] \frac{n_{v^*}}{n_{v_{\text{eq}}}} \\ &= k_{d_{\text{eq}}}[T] \exp\left[\epsilon_v \left(\frac{1}{T} - \frac{1}{T_v}\right)\right] \frac{Z_{\text{vib}}[T]}{Z_{\text{vib}}[T_v]} \end{aligned} \tag{21}$$

A simple weak-bias model may be constructed by assuming that

$$k_{d_v} = k_0[T] \exp[-(D - \epsilon_v)/T] \tag{22}$$

where the value of k_0 is established by requiring consistency with the equilibrium rate coefficient:

$$k_0[T] = Z_{\text{vib}}[T] k_{d_{\text{eq}}}[T] \frac{\exp(D/kT)}{(v^* + 1)} \tag{23}$$

Substitution for k_{d_v} yields the following for this weak-bias form:

$$k_{d_{\text{eff}}}[T, T_v] = \frac{k_{d_{\text{eq}}}[T]}{(v^* + 1)} \frac{Z_{\text{vib}}[T]}{Z_{\text{vib}}[T_v]} N_{\text{tot}} \sum_{v=0}^{v^*} \exp\left[\epsilon_v \left(\frac{1}{T} - \frac{1}{T_v}\right)\right] \tag{24}$$

The state-specific dissociation rates compete with the V-V and V-T rates and the state populations are depleted in the excitation phase. The current paper shows the nonequilibrium dissociation rate coefficients for the bounds of strong and weak biases for dissociation in a heat bath with temperatures of 5000, 10,000, and 20,000 K. These bounds of strong- and weak-bias dissociation rate coefficients are compared with available experimental fits in [9] to identify the trends in vibrational bias at different temperatures.

The probability of the collision process for the FHO consists of exerting a perturbing force on the assumed harmonic oscillator model of the molecule and is written as (see, for example, [10])

$$\begin{aligned} &P_{\text{VRT}}(i \to f, Q) \\ &\quad = i! f! Q^{i+f} \exp(-Q) X \left| \sum_{r=0}^{n} \frac{(-1)^r}{r!(i-1)!(f-r)!} \frac{1}{Q^r} \right|^2 \end{aligned} \tag{26}$$

where subscript VRT denotes vibration–rotation–translation energy transfer, $n = \min(i, f)$, and $Q = (\Delta E/\hbar\omega)$ is the dimensionless energy transferred to the initially nonvibrating classical oscillator in an *AB–M* collision.

The total probability of collisional dissociation from vibrational level i is therefore a sum over all final dissociative vibrational levels:

$$P_{\text{diss}}(i) = \sum_{E_f \geq D} P_{\text{VRT}}(i \to f) \tag{27}$$

Improvements to the FHO model discussed in [10,31] include symmetrization of the collision velocity to enforce detailed balancing, accounting for anharmonicity of the oscillator potential curve using an average frequency, generalization for vibration–vibration–translation transitions (both nonresonant and between different species) and generalizations of the FHO model to noncollinear collisions.

The state-specific rate coefficients based on the FHO-based dissociation model and from the semiclassical theory of dissociation developed by Macheret and Adamovich [9] give the dissociation rate as

$$k_{\text{diss}}(v, T) = \left(\frac{8kT}{\pi m}\right)^{0.5} \int_0^\infty \sigma_{\text{diss}}(v, U, T) \exp\left(-\frac{U}{T}\right) \mathrm{d}\left(\frac{U}{T}\right) \tag{28}$$

where the expression for the dissociation cross section assuming free-rotation approximation of diatom–atom collision is

$$\begin{aligned} &\sigma_{\text{diss}}(i, E, T) \\ &\quad \approx \pi R_m^2 \left(\frac{E}{T}\right)^2 \frac{1}{\pi^2} \int_0^1 \mathrm{d}y \int_0^1 \mathrm{d}\epsilon \int_0^\pi \mathrm{d}\vartheta \int_0^\pi \mathrm{d}\varphi \sum_f P_{if}(E, \epsilon, \vartheta, \varphi, y) \end{aligned} \tag{29}$$

and for the diatom–diatom collision is

$$\sigma_{\text{diss}}(i, E, T) \approx \pi R_m^2 \left(\frac{E}{T}\right)^3 \frac{1}{\pi^4} \int_0^1 \mathrm{d}y \int_0^1 \mathrm{d}\epsilon_1 \int_0^1 \mathrm{d}\epsilon_2 \int_0^\pi \mathrm{d}\vartheta_1 \int_0^\pi \mathrm{d}\vartheta_2 \int_0^\pi \mathrm{d}\varphi_1 \int_0^\pi \mathrm{d}\varphi_2 \sum_f P_{if}(E, \epsilon_1, \epsilon_2, \vartheta_1, \vartheta_2, \varphi_1, \varphi_2, y) \tag{30}$$

E. State-Specific Vibrational and Dissociation Kinetics

Consider diatomic molecules AB colliding with atoms M, with the consequence of the vibrational energy state of the molecule changing from i to f:

$$AB(i) + M \to AB(f) + M \tag{25}$$

The state-specific V-T and dissociation rate coefficients were generated from the energy-transfer probabilities from the nonperturbative FHO-based model using a three-dimensional semiclassical analytic model of vibrational energy transfer, given by Adamovich and Rich [10]. The model is based on the analysis of classical trajectories of a free-rotating molecule acted upon by a superposition of repulsive exponential atom-to-atom potentials. The energy-transfer probabilities from this model achieved good agreement with the results of three-dimensional close-coupled semiclassical trajectory calculations using the same potential energy surface.

In the above, ϵ, ϑ, and φ are the fractional rotational energy, rotational angle, and angular momentum vector, respectively; E is the total collision energy; U is the potential energy for the 3-D molecule–molecule collisions; P_{if} is the probability of the transition process; y is a function of the impact parameter; R_m is the hard-sphere diameter; i is the index of the initial vibrational quantum level; and v is the index of the quantum level. The above equations were derived by evaluating the probabilities of vibrational transitions including dissociation by determining a potential energy surface and then integrating the classical equations of motion for the system (see [4,5,9]).

A Monte Carlo integration was performed to solve Eqs. (29) and (31), details of which are given in [4,5]. The multidimensional Monte Carlo integration was implemented by repeated subroutine calls to a one-dimensional random number generator by using a different seed each time. The primary reason is to avoid any hidden intrinsic correlations in the phase space. Thus, each subroutine call returns a random value for use as a given parameter of the phase space

Table 1 Approaches to computational modeling

Model[a]	Vibration	Dissociation	Clock time[b]
Full dissociation	State-specific 48 levels (FHO-based)	State-specific 48 levels (FHO-based)	72 h
Vibration–dissociation coupling with depletion model	Landau–Teller [28] (Millikan–White [29] relaxation times)	Depletion factors derived from state-specific 48 levels (FHO-based)	5 min
No dissociation	State-specific 48 levels (FHO-based)	None	4 h
Park [22] dissociation (for reference)	Landau–Teller [28] (Millikan–White [29] relaxation times)	Geometric mean T, T_v	5 min

[a]Computation times for full-dissociation model and no-dissociation models include dynamic state-to-state calculations of V-T rate coefficients. State-specific dissociation rate coefficients for the full-dissociation model is implemented as table lookup.
[b]Wall-clock time is based on computations of Mach 19.83 flow past a 2-D/axisymmetric blunt body on a 3.2 GHz quad-core Intel Xeon processor.

and also returns a random seed for the random generation of the next parameter. Thus, a parameter phase-space point of eight or more dimensions is created. The process is continued to generate the next phase-space point. In the present study, a database of dissociation rate coefficients for N_2–N_2 and N_2–N collisions was generated for temperatures up to 25,000 K by performing the Monte Carlo integrations.

III. Conditions of Numerical Simulation

A Mach 19.83 nitrogen flow past a hemisphere cylinder was considered in this study. The maximum shock temperature was 21,000 K and the dissociation reaction for the nitrogen molecule considered was

$$N_2 + M \rightleftharpoons 2N + M \tag{31}$$

The radius of the hemisphere was 0.1524 m. Freestream pressure and temperature were 27 Pa and 300 K, respectively. Four different approaches to modeling dissociation were considered. The first approach, which is the most rigorous, incorporates FHO-based state-specific V-T rate coefficients [10] and dissociation rate coefficients [9] into a solution of the master kinetic equations coupled to the fluid dynamic equations (1–4). The master kinetic equations consisted of state-specific vibration and dissociation rates in 48 vibrational quantum levels. As a first step toward implementation of the full state kinetic dissociation rates into the fluid dynamics equations, the recombination process was neglected.

The second approach implements the nonequilibrium depletion factor based on FHO-based V-T state kinetic rates to define the nonequilibrium dissociation rate; an earlier section on the depletion model provides information on the derivation of the depletion factor.

The third approach does not allow dissociation to occur, but considers only the exchanges in the vibrational–translational energy. Here, the FHO-based state-specific V-T rate coefficients are used.

The fourth approach, for reference purposes, uses the Landau–Teller [28] form of modeling V-T energy transfers and the Park two-temperature model [22] for dissociation. Table 1 summarizes these four modeling approaches and their corresponding wall-clock times.

The numerical algorithm employed to solve the coupled set of equations is the Roe flux difference method with entropy correction used in [23]. An explicit predictor–corrector method is used to advance the solution in time. The numerical computation of the most rigorous model of the full dissociation takes a considerably longer time than the simplified models (Table 1), due to the numerical stiffness associated with the source terms of Eq. (1).

IV. Results and Discussion

Results are presented in two sections. The first section presents the state-specific V-T and dissociation rates and the comparison with global equilibrium rates. Also shown in this section are the sensitivity of V-T rates on depletion and the effect of V-T rates on vibrational bias for dissociation temperatures up to 25,000 K. The second section shows the effect of coupling the nonequilibrium vibration and dissociation kinetics with a Mach 19.83 nitrogen flow past a blunt body.

A. Depletion Factors and Vibrational Bias in Dissociation

Figures 2 and 3 depict the state-specific dissociation rate coefficients of N_2–N_2 and N_2–N collisions, respectively, at temperatures of 6100, 10,000, 15,100, 21,100, and 25,300 K, calculated with the FHO-based dissociation model of Macheret and Adamovich [9]. At all temperatures considered, the rate coefficient is highest in the upper vibrational levels. The rate coefficients in the upper states for N_2–N collisions are similar in magnitude to those of N_2–N_2 collisions. In the lower energy states, however, the rate coefficients for N_2–N are a few orders of magnitude less than the corresponding rate coefficients for N_2–N_2 collisions across the range of temperatures (6100 to 25,300 K) considered. Figures 4 shows the equilibrium global dissociation rate coefficient calculated from the state-specific dissociation rate coefficients of N_2–N_2 collisions,

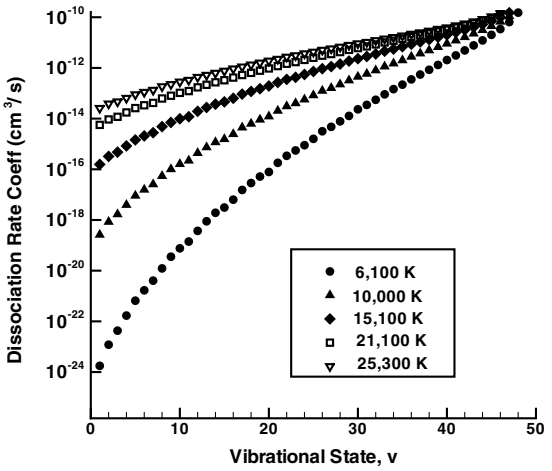

Fig. 2 State-specific dissociation rate coefficient for N_2–N_2 collisions from FHO-based dissociation model [9].

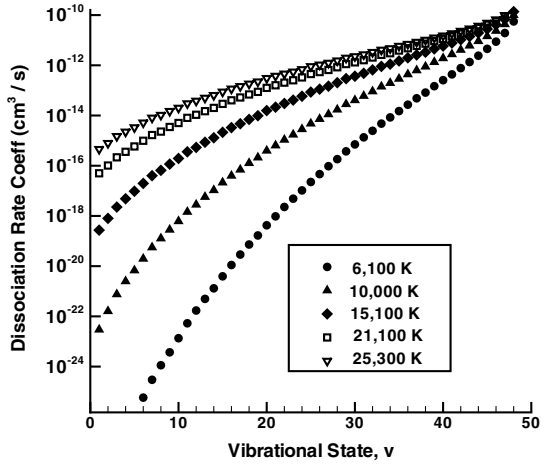

Fig. 3 State-specific dissociation rate coefficient for N_2–N collisions from FHO-based dissociation model [9].

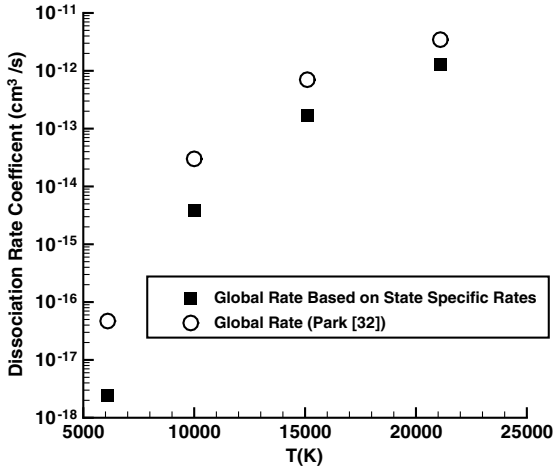

Fig. 4 Comparison of equilibrium global dissociation rates of N_2–N_2 based on FHO-based state-specific and Park global rates [32].

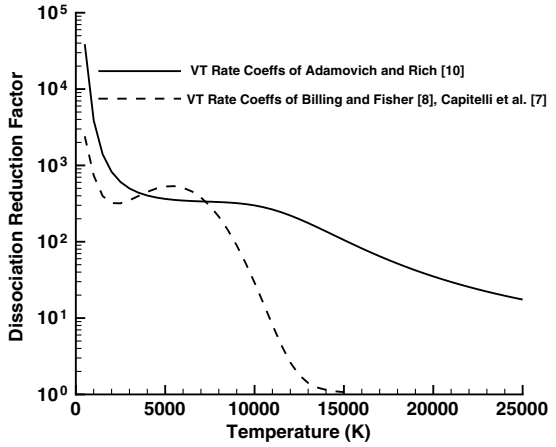

Fig. 6 Nonequilibrium dissociation rate: Vibrational population depletion-induced dissociation reduction factor from equilibrium dissociation rates for two sets of state-specific V-T rate constants. The Billing and Fisher [8] and Capitelli et al. [7] rate coefficients were implemented using curve-fit expressions of [24].

compared with those from [32]. The global rate coefficient for dissociation was obtained by

$$k_d(\text{global}) = \sum \frac{\text{N}_2[v]k_d[v]}{\text{N}_2} \tag{32}$$

It is seen that the equilibrium global dissociation rate coefficients are similar to [32], but lower by a factor ranging from 2 to 10.

Figure 5 depicts the variation in V-T deexcitation rate coefficients from 1) Adamovich and Rich [10] and 2) expressions proposed in [24] for rate coefficients of Billing and Fisher [8] and Capitelli et al. [7]. At the lower temperatures of 1000 and 5000 K (Fig. 5a), the rate coefficients from the two sources have small differences. At higher temperatures, however, the Billing and Fisher [8] and Capitelli et al. [7] rate coefficients (shown at temperatures of 15,000 and 20,000 K in Fig. 5b) are orders of magnitude higher and clearly show an out-of-range error in the curve-fit expressions [24] intended to obtain these rate coefficients. Described next is the effect of these two sets of V-T rate coefficients on the amount of vibrational population depletion occurring under dissociating temperatures for nitrogen.

A model to calculate a factor for depletion of vibrational population due to dissociation from the last level was presented in [25,30]. The factor presented as a ratio of the nonequilibrium-to-equilibrium dissociation rate finds use as a vibration–dissociation coupling model in hypersonic codes. This factor gives insight into the role of the relative time scales of vibrational relaxation and dissociation for a range of temperatures typically encountered in shock-layer flows. Figure 6 shows the dissociation reduction factor from an equilibrium dissociation rate.

The reduction factor is obtained for the two sets of V-T rate coefficients given by 1) curve-fit expression [24] of Billing and Fisher [8] and Capitelli et al. [7] and 2) Adamovich and Rich [10]. Both sets of V-T rates show high depletion at temperatures below 10,000 K. However, above 10,000 K, where dissociation is expected to be high, the depletion curve with V-T rate coefficients from the curve-fit expression [24] of Billing and Fisher [8] and Capitelli et al. [7] V-T rates approaches 1 at 15,000 K, meaning that there is no more depletion at this temperature. The out-of-range error is not unexpected and the goal of the present study is to study the sensitivity of the depletion factor to the aforementioned curve-fit expressions. For temperatures higher than 15,000 K, the rate coefficients from the curve-fit expression of Billing and Fisher [8] and Capitelli et al. [7]. V-T rate coefficients do not cause further depletion to occur; however, the FHO-based V-T rate coefficients from Adamovich and Rich [10] cause large population depletion at temperatures beyond 15,000 K. At the highest temperature of 25,000 K shown, the dissociation reduction factor from its equilibrium rate using the V-T rate coefficients of Adamovich and Rich is 18.

Figure 7 shows the ratio of nonequilibrium-to-equilibrium population density obtained from the two sets of V-T rate coefficients 1) from curve-fit expression [24] of V-T rate coefficients of Billing and Fisher [8] and Capitelli et al. [7] and 2) Adamovich and Rich [10]) at various temperatures, the effect of depletion in the vibrational

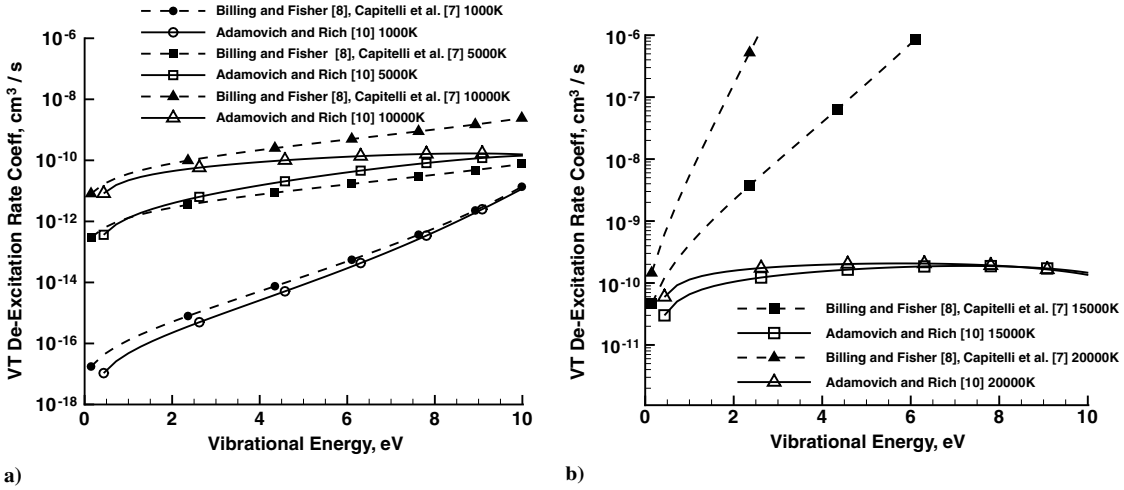

Fig. 5 Comparison of V-T rate coefficients from Adamovich and Rich [10] and curve-fit expression of rate constants of Billing and Fisher [8] and Capitelli et al. [7]: a) $T = 1000$, 5000, and 10,000 K and b) $T = 15,000$ and 20,000 K.

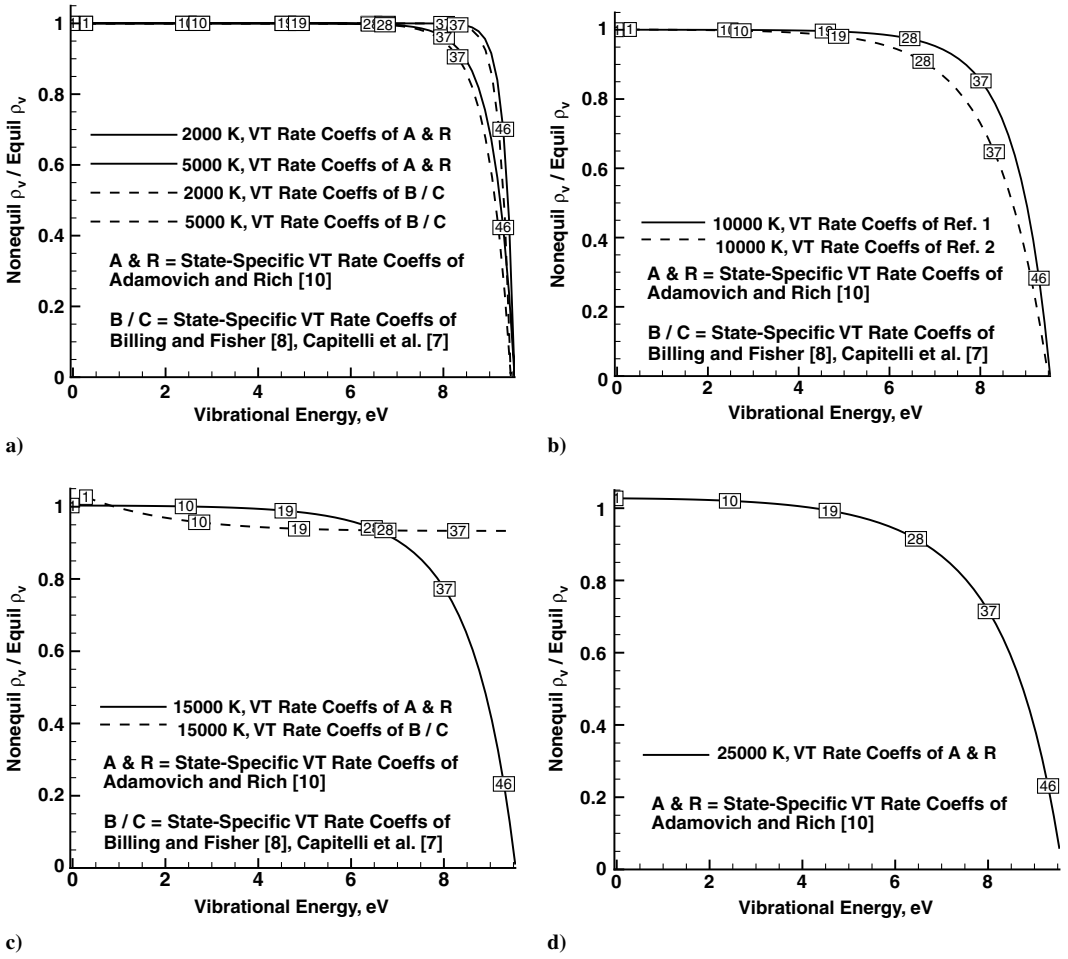

Fig. 7 Ratio of population distribution showing effect of vibrational population depletion in vibrational quantum levels: a) 2000 and 5000 K, b) 10,000 K, c) 15,000 K, and d) 25,000 K. The Billing and Fisher [8] and Capitelli et al. [7] rate coefficients were implemented using curve-fit expressions of [24].

manifold due to all of the dissociation occurring only from the last level. At the lower temperatures of 2000 and 5000 K (Fig. 7a) the two sets of rates depict similar depletion effects occurring in the upper levels from 37 to 48. However, dissociation in nitrogen at these lower temperatures is expected to be small. At a temperature of 10,000 K (Fig. 7b) the depletion from both sets of V-T rates begins in the intermediate level 19 and increases to the last level of 48. At this temperature, the ratio of population density of the nonequilibrium to equilibrium is lower for the V-T rate coefficients from the curve-fit expression of Billing and Fisher [8] and Capitelli et al. [7] V-T rate coefficients. At 15,000 K (Fig. 7c) there is insignificant depletion for the Billing and Fisher [8] and Capitelli et al. [7] V-T rate coefficients, but there is considerable depletion in the upper levels from the Adamovich and Rich [10] V-T rate coefficients. For the highest temperature of 25,000 K shown in Fig. 7d, there is significant depletion in the upper levels (the depletion curve for V-T rate coefficients from the curve-fit expression of Billing and Fisher [8] and Capitelli et al. [7] V-T rate coefficients is not shown, due to depletion being insignificant). The effect of these differences in the magnitude of depletion due to different V-T rate coefficients will be shown later on the blunt-body shock standoff distance.

The results of the vibrational bias model for the gas temperatures of 5000, 10,000, and 20,000 K in a heat bath is shown in Fig. 8. These temperatures are representative of the shock wave flow to be discussed next. Recall from an earlier section that the strong-bias model considers dissociation from the last level only, whereas the weak-bias model contributes to the global dissociation rate with equal probability from any vibrational levels. The calculated two-temperature dissociation rate constant $k_{d_{\text{eff}}}(T, T_v)$ is for the case of a nitrogen bath at the various gas temperatures. The comparison of different biases yield large differences at vibrational temperatures far from equilibrium. At $T \gg T_v$, the rate coefficients of strong-bias model are several orders of magnitude lower than those of the weak-bias model. At gas temperatures of $T = 5000$ and 10,000 K, the strong-bias model yields comparable rate constants with the experimental fit (taken from [9]) than the weak-bias model. At $T = 20,000$ K, however, the weak-bias model has a better match with the experimental data. These results lead to a better understanding of the effect of bias due to the inclusion of distributed dissociation (as in the full state-specific dissociation model) to be described next.

B. Vibration and Dissociation Kinetics on a Mach 19.83 Flow Past a Body

High-Mach-number blunt-body flow solutions were investigated to assess the effects of the state-specific dissociation rates on the thermochemical relaxation phenomenon. The state-specific vibration and dissociation rate constants implemented via the master kinetic equations were coupled to the fluid dynamic equations, and results are presented for translational and first-level vibrational temperatures, mass fractions, and populations distributions in the shock layer of the blunt-body flowfield.

Figures 9 and 10 show comparisons of the translational temperature contours of the full-dissociation model with 1) Park [22] two-temperature dissociation model and 2) the depletion model. The primary differences seen in the contours between the three models are discussed for the temperature profiles along the stagnation streamline in Figs. 11 and 12. Figures 11 and 12 show the translational and first-level vibrational temperatures variation along the stagnation streamline for different cases considered in the study: 1) the full-dissociation model with state-specific FHO-based V-T

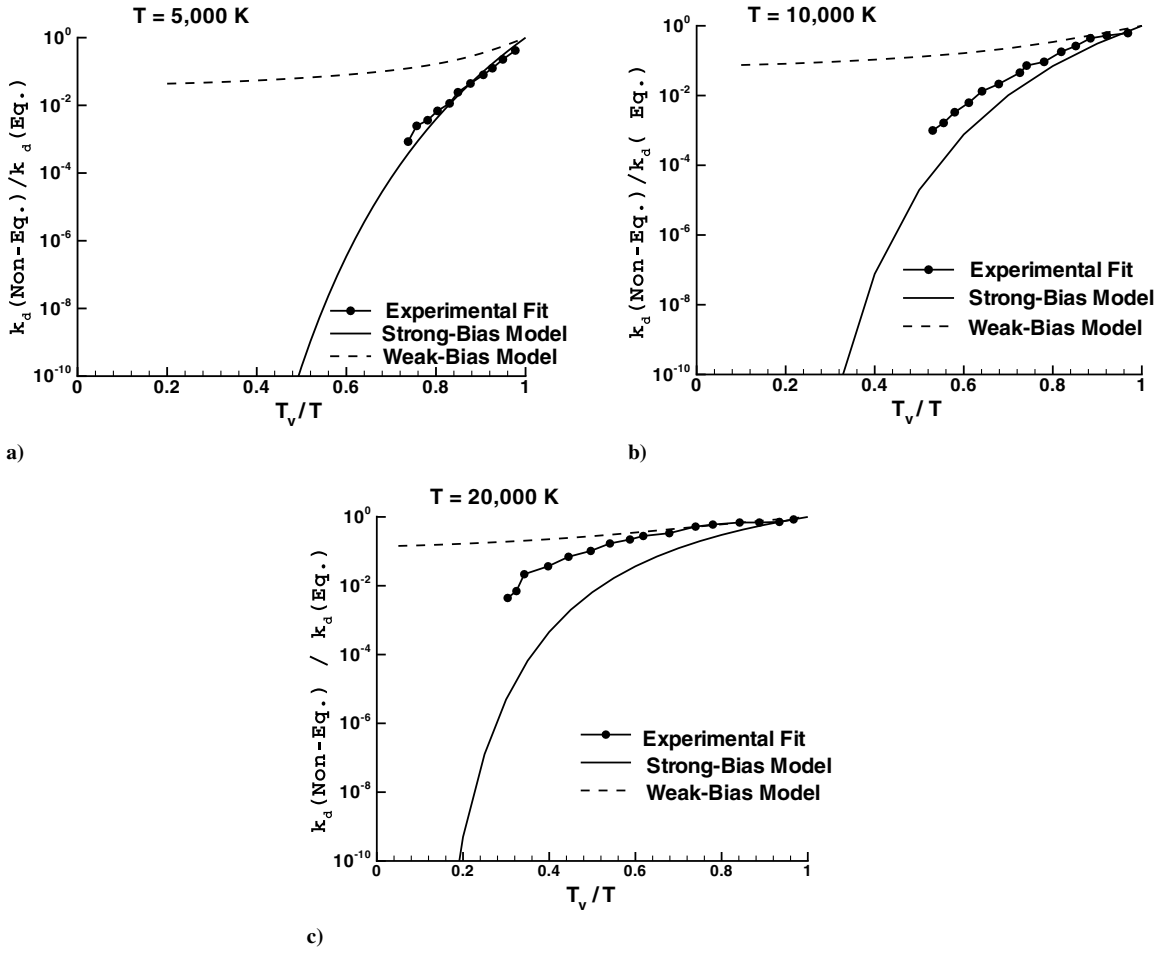

Fig. 8 Dissociation rate coefficient for weak- and strong-bias models in a heat bath: a) 5000 K, b) 10,000 K, and c) 20,000 K.

[10] and dissociation rates [9]; 2) Landau–Teller vibrational relaxation model [28] with the two-temperature Park dissociation model [22]; 3) state-specific FHO-based V-T rates [10] without dissociation; and 4) Landau–Teller [28] vibrational relaxation model [28] with dissociation simulated by the depletion model with two sets of state-specific V-T rate constants, curve-fit expression [24] of Billing and Fisher [8], Capitelli et al. [7], and Adamovich and Rich [10]. See Table 1 for a summary of the modeling approaches.

The comparison of translational temperatures given by the full-dissociation model with the simplified Landau–Teller [28] vibration model with Millikan and White [29] relaxation times and Park [22] two-temperature dissociation rates is shown in Figs. 11a. The simplified model shows a much greater dissociation than the full-dissociation model, resulting in a much smaller shock standoff distance. The shock standoff distance by the simplified model is 24% less than the full-dissociation model.

Figure 11b shows the translational temperature predicted by the full-dissociation model compared with the no-dissociation case with vibrational exchanges occurring with the state-specific V-T rate coefficients from the FHO-based model of Adamovich and Rich

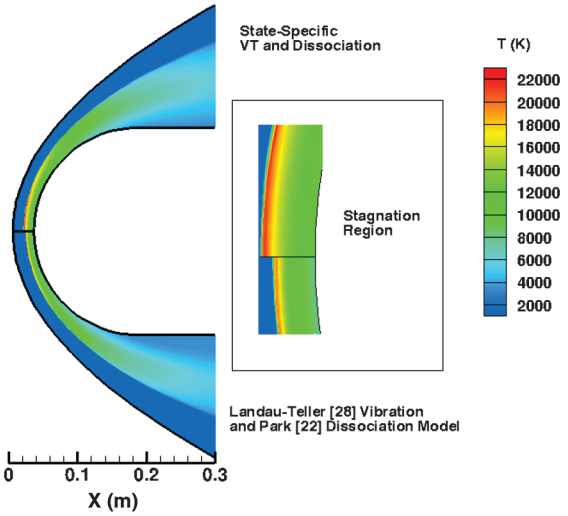

Fig. 9 Translational temperature contours comparing full-dissociation model with Park [22] dissociation model.

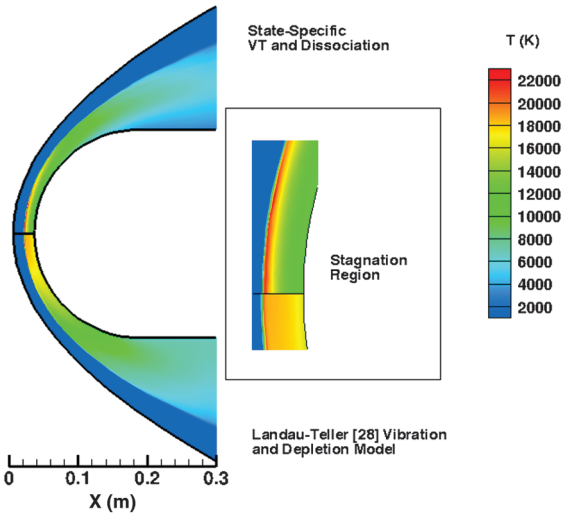

Fig. 10 Translational temperature contours comparing full-dissociation model with depletion model.

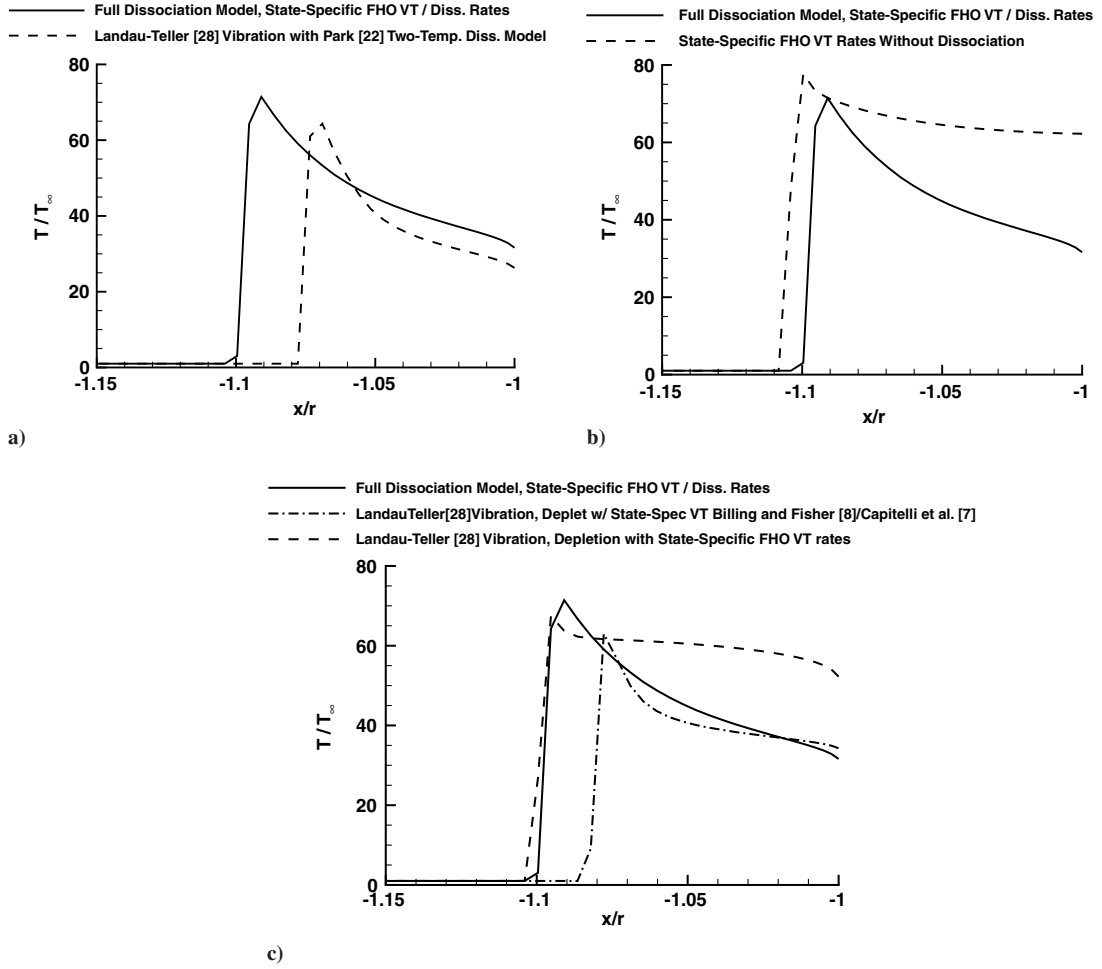

Fig. 11 Effect of nonequilibrium kinetics in blunt-body flow: variation of translational temperature in the shock layer ($M_\infty = 19.83$, $p_\infty = 27$ Pa, $T_\infty = 300$ K, and $r = 0.1524$ m): a) full-dissociation model compared with Park [22] dissociation model, b) full-dissociation model compared with case of V-T exchanges only but no dissociation, c) full-dissociation models compared with depletion models. Note that $X/r = -1$ is at the body and $X/r = -1.15$ is at the freestream.

[10]. Since dissociation is endothermic, there is reduction in shock standoff distance and a lowering of temperature in the shock layer, with the temperatures approaching equilibrium conditions (see also Fig. 12) as the flow stagnates at the body.

Figures 11c shows translational temperature along the stagnation streamline of the full-dissociation model compared with those of the depletion model. shock standoff distance predicted by the depletion model with the state-specific V-T rates of FHO-based model of Adamovich and Rich [10] matches that of the full-dissociation model; however, higher temperatures are predicted in the shock layer compared with the full-dissociation case, due to high depletion at the shock-layer temperatures. The depletion model with V-T rate coefficients in the curve-fit expression [24] of Billing and Fisher [8] and Capitelli et al. [7] V-T rate coefficients predicts a much lower shock standoff distance compared with the full-dissociation model and the depletion model with FHO-based Adamovich and Rich [10] V-T rate coefficients. The high V-T rates from the curve-fit of the Billing and Fisher [8] and Capitelli et al. [7] V-T rates at the shock temperatures (Fig. 5), and the consequent reduction in depletion (Figs. 6 and 7) is attributed to the lowering of the shock standoff distance by 18%, compared with that of the full-dissociation case.

The first-level vibrational temperatures for the full-dissociation model and the Landau–Teller [28] vibration model with Park [22] dissociation model shown in Fig. 12a are related to the translational temperature discussed in Fig. 11a, as a consequence of V-T energy exchanges; the greater peak translational temperature for the full-dissociation case has a corresponding reduced peak first-level vibrational temperature but a greater shock standoff distance. The first-level vibrational temperature for the no-dissociation case (Fig. 12b) is higher than for the full-dissociation case, as expected. The first-level vibrational temperatures for the full-dissociation case and the depletion cases show large variations with each other (Fig. 12c), similar to the translational temperature variations; the vibrational temperature predicted by the depletion model with FHO-based V-T rates is the highest, indicating the least amount of population depletion in the vibrational levels.

Figure 13 shows the mass fraction of diatomic and atomic nitrogen along the stagnation streamline for the three cases considered in this study. The full-dissociation model predicts a lower mass fraction of diatomic nitrogen than the depletion model. The high degree of dissociation by the Park [22] two-temperature dissociation model is evident by the sharp reduction in mass concentration of diatomic nitrogen in the shock layer.

The implementation of state-specific dissociation rate coefficients coupled to fluid dynamic equations allows us to assess the effect of vibrational bias on dissociation for the given Mach 19.83 blunt-body flowfield. The state-specific vibration and dissociation frequencies given by the product of their respective population densities and rate coefficients are shown in Figs. 14 and 15, respectively. The figures show the frequency with respect to the vibrational quantum levels for four different translational temperatures along the stagnation streamline: the lowest temperature near the body and the highest near the shock wave. The populations shown are for both real (non-equilibrium in the flowfield) and equilibrium populations to assess the deviation of the nonequilibrium population in the Mach 19.83 flowfield from its equilibrium value.

Figure 14 shows the state-specific vibrational frequency for the shock-layer temperatures for V-T energy exchanges, but in the

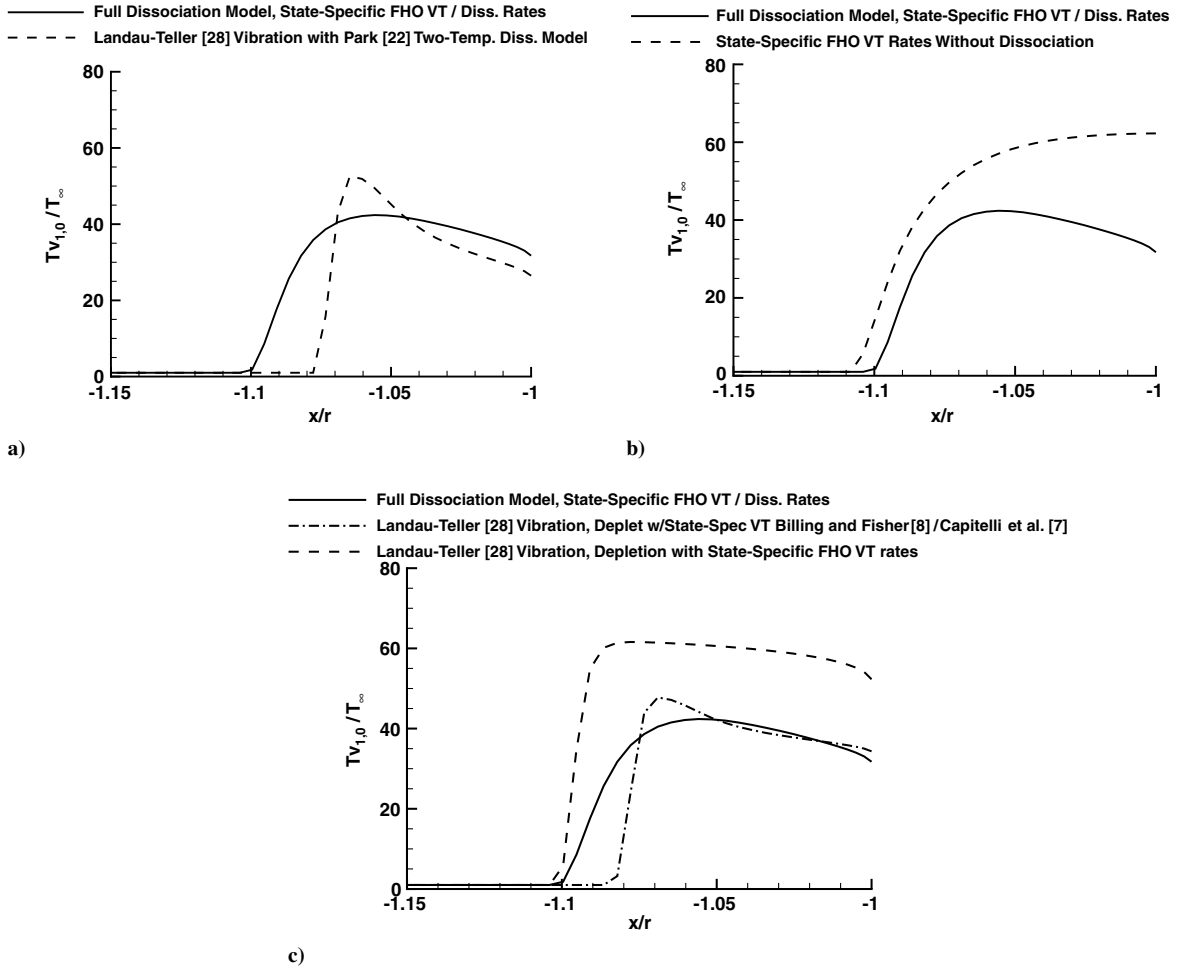

Fig. 12 Effect of nonequilibrium kinetics in blunt-body flow with variation of first-level (1,0) vibrational temperature in the shock layer ($M_\infty = 19.83$, $p_\infty = 27$ Pa, $T_\infty = 300$ K, and $r = 0.1524$ m) for full-dissociation model compared with a) Park [22] dissociation model, b) case of V-T exchanges only but no dissociation, and c) depletion models. Note that $X/r = -1$ is at the body and $X/r = -1.15$ is at the freestream.

absence of dissociation to assess the effect of vibrational bias and depletion. The shock-layer temperatures in the absence of dissociation vary from 18,942 K near the body to 23,303 K near the shock wave. Note that at the lower temperature of $T = 18,942$ K in the stagnation region (Fig. 14a), the nonequilibrium rate is closer to the equilibrium rate along most of the quantum levels. However, with increase in translational temperatures in the shock layer (Figs. 14b–14d), the difference between the nonequilibrium rate of the Mach 19.83 flow and the equilibrium rate increases, with the peaks lying under $v = 10$. The difference is attributed to the inability to populate the higher vibrational levels with increase in temperature along the stagnation streamline for this high-Mach-number flow.

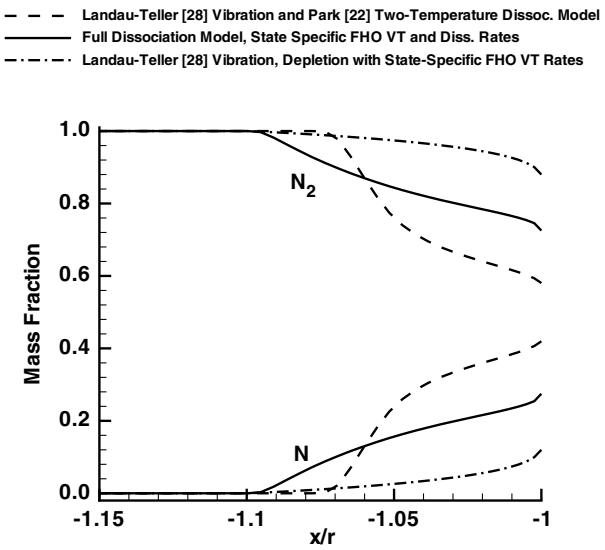

Fig. 13 Blunt-body flow: Mass fraction along the stagnation streamline ($M_\infty = 19.83$, $p_\infty = 27$ Pa, $T_\infty = 300$ K, and $r = 0.1524$ m). Note that $X/r = -1$ is at the body and $X/r = -1.15$ is at the freestream.

Figure 15 shows similar effects as above, but for the case where there is dissociation from all the vibrational quantum levels. Because of dissociation, the shock-layer temperatures are lower than the above and are between 9000 to 21,000 K along the stagnation streamline, with the highest temperature in the postshock region and the lowest temperature near the body. The product of population densities and dissociation rate coefficients is normalized for the equilibrium and nonequilibrium (Mach 19.83 flow simulation) with their respective highest (peak) values. Note that at all the temperatures in the shock layer, the equilibrium population shows a strong bias to dissociation; however, the nonequilibrium rates are such that dissociation primarily occurs from the lower energy states (weak bias); the peak contribution from $v = 26$ at the lower temperature of $T = 9479$ K in the stagnation region, and $v = 1$ at the highest temperature of 21,426 K near the shock wave. The contribution of the lower energy levels to dissociation is attributed to the partial heating of the vibrational manifold due to V-T energy exchanges. It is concluded that the full dissociation for the Mach 19.83 flow favors a weak vibrational bias, with dissociation occurring primarily from low-to-intermediate vibrational quantum levels. This observation is consistent with the favoring of a weak bias at the high temperature given by the experimental fit in Fig. 8.

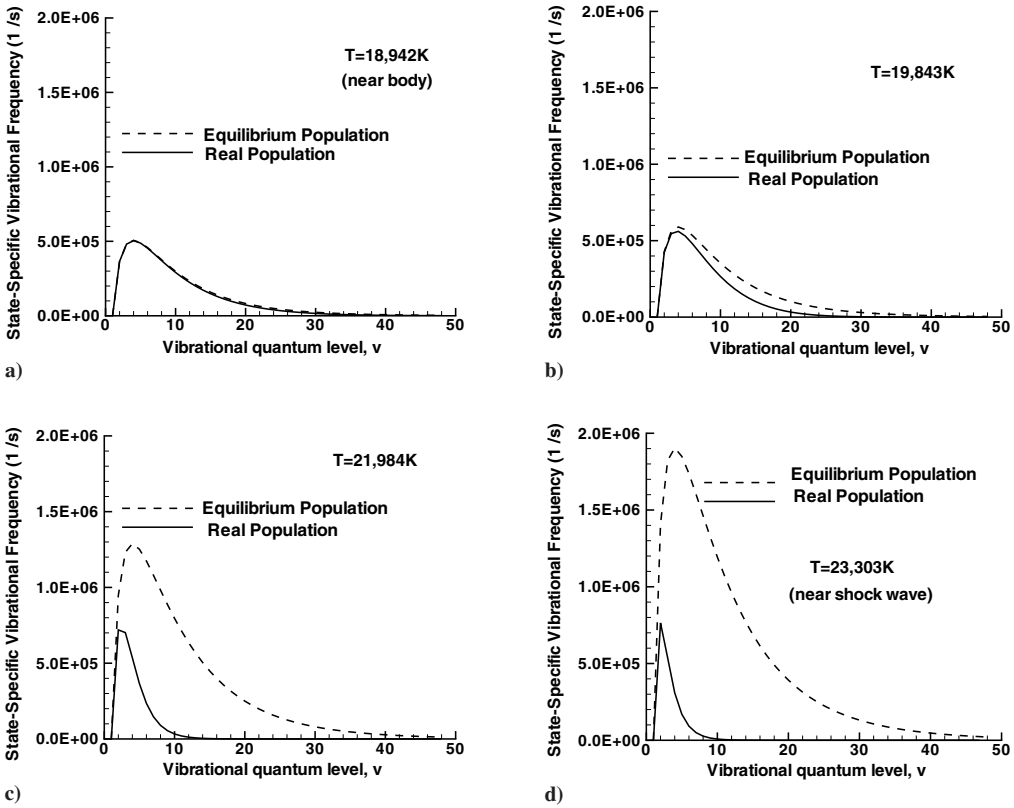

Fig. 14 Blunt-body flow with no dissociation for product of vibrational population and rate coefficient along stagnation streamline ($M_\infty = 19.83$, $p_\infty = 27$ Pa, $T_\infty = 300$ K, and $r = 0.1524$ m:) a) $T = 18,942$ K, b) $T = 19,843$ K, c) $T = 21,984$ K, and d) $T = 23,303$ K. Figure shows the magnitude of heating of the vibrational manifold due to V-T energy exchanges in the absence of dissociation. Real population is the actual nonequilibrium population in the flowfield.

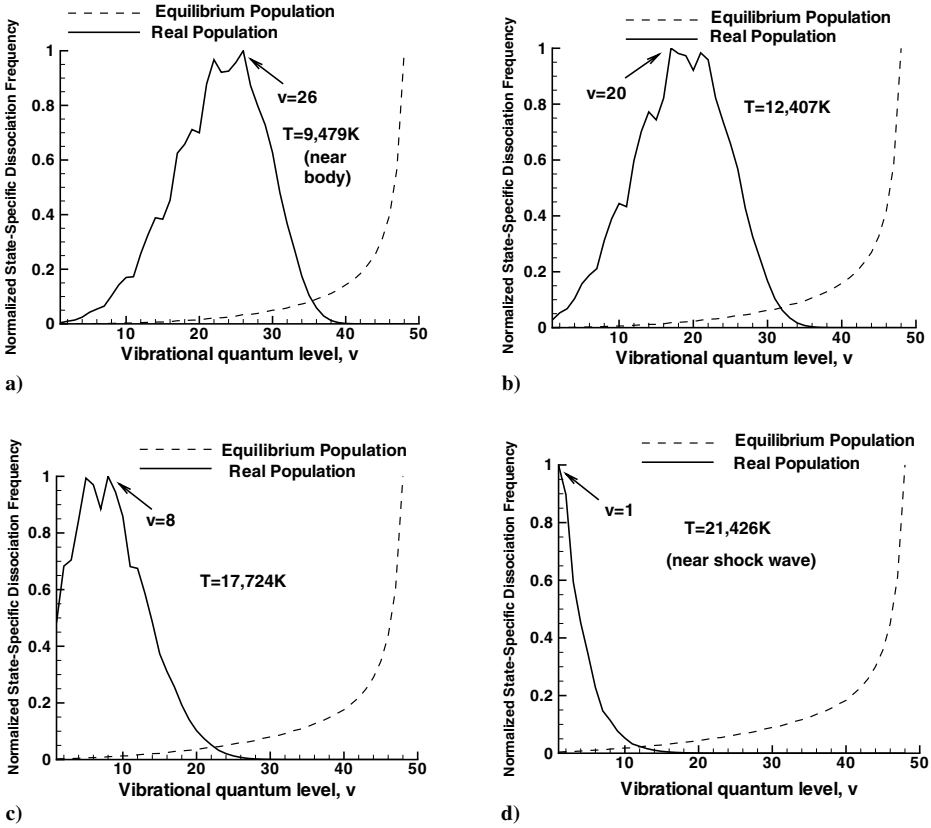

Fig. 15 Blunt-body flow with the full-dissociation model for product of vibrational population and dissociation rate coefficient (normalized by highest value) along stagnation streamline ($M_\infty = 19.83$, $p_\infty = 27$ Pa, $T_\infty = 300$ K, and $r = 0.1524$ m): a) $T = 9,479$ K, b) $T = 12,407$ K, c) 17,724 K, and d) 21,426 K. Figure shows the heating rate of the vibrational manifold and the quantum levels from which dissociation occurs. Real population is the actual nonequilibrium population in the flowfield.

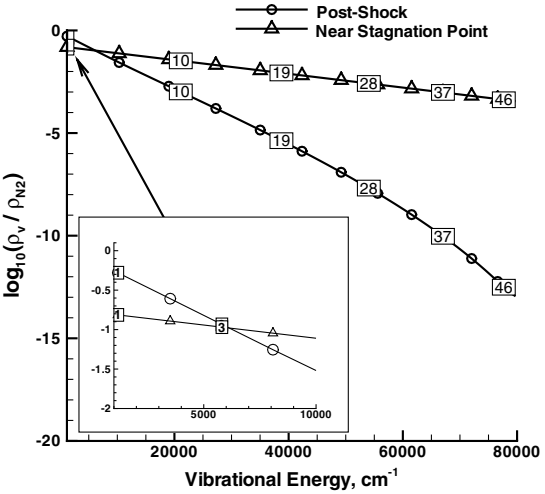

Fig. 16 Blunt-body flow with no dissociation for population distribution in the vibrational levels at two locations in the shock layer ($M_\infty = 19.83, p_\infty = 27$ Pa, $T_\infty = 300$ K, and $r = 0.1524$ m).

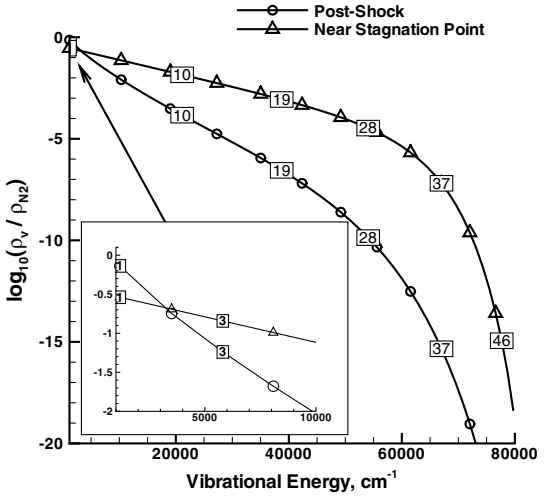

Fig. 17 Blunt-body flow with dissociation from all vibrational quantum levels: Population distribution in the vibrational levels at two locations in the shock layer ($M_\infty = 19.83, p_\infty = 27$ Pa, $T_\infty = 300$ K, and $r = 0.1524$ m).

The above-mentioned observations are further supported by the population distributions in the shock layer for Mach 19.83 flow with and without dissociation in Figs. 16 and 17, respectively. The case of no dissociation shown in Fig. 16 depicts Boltzmann distributions at the two locations in the shock layer: the postshock ($T = 23,303$ K) and near the body ($T = 18,942$ K). The population distribution for the Mach 19.83 flow with full dissociation is shown in Fig. 17. At the two locations, one in the postshock ($T = 9479$ K) and the other near the stagnation point ($T = 21,426$ K), it is seen (Fig. 17) that the population distributions are highly non-Boltzmann and there is greatly reduced population with increase in vibrational quantum levels, due to the partial heating of the vibrational manifold mentioned earlier. The close-up inset figures show the detail near the ground-state energy. The population reduction in the upper levels (Fig. 17) is far greater than can be attributed to depletion; the depletion factor (nonequilibrium dissociation reduction factor from its equilibrium rate) is 300 at $T = 10,000$ K (see Fig. 6).

V. Conclusions

State-specific vibration and dissociation rate coefficients were incorporated into a solution of the master kinetic equations coupled to fluid dynamic equations to perform computational simulation of a Mach 19.83 nitrogen flow past a hemisphere cylinder. The state-specific dissociation rate coefficients of N_2–N_2 collisions and N_2–N collisions in 48 vibrational quantum levels based on the semi-classical theory were taken from the literature. A set of global dissociation rate coefficients based on the state-specific rate coefficients were compared with those available in the literature. The global dissociation rate coefficient was a factor of 2–10 lower.

The sensitivity studies on the effect of two different sets of V-T rate coefficients on population depletion in nitrogen dissociation showed that the FHO-based rates cause high depletion in the temperature range of 15,000 to 25,000 K, whereas the depletion with curve-fit expression of Billing and Fisher [8] and Capitelli et al. [7] V-T rate coefficients was negligible beyond 15,000 K.

A Mach 19.83 flow past a hemisphere cylinder was simulated with three different dissociation models: 1) the solution of the master kinetic equations using state-specific vibration and dissociation, 2) the depletion model based on detailed vibrational kinetics, and 3) the Landau–Teller [28] vibrational relaxation and Park [22] two-temperature dissociation model. The shock standoff distance of the Park model differs from the full-dissociation model by 24%. The shock standoff distance predicted by the depletion model using FHO-based V-T rate coefficients matched that of the full-dissociation case; however, the depletion model is derived with the assumption that the flow residence time is much longer than the relaxation time, which might make it invalid in nonequilibrium flow regimes where the residence times are small.

Coupling the state-to-state vibration and dissociation kinetics with the Mach 19.83 blunt-body flowfield revealed that the low-to-intermediate vibrational levels were the primary contributors to the global dissociation. This observation is consistent with the experimental fits supporting a weak vibrational bias to dissociation.

Acknowledgments

This research was supported under U.S. Air Force Office of Scientific Research contracts monitored by F. Fahroo and J. Schmisseur. FORTRAN subroutines to generate state-specific vibration and dissociation rate coefficients were provided by I. Adamovich.

References

[1] Sarma, G. S. R., "Physico-Chemical Modelling in Hypersonic Flow Simulation," *Progress in Aerospace Sciences*, Vol. 36, 2000, pp. 281–349.
doi:10.1016/S0376-0421(00)00004-X

[2] Orsini, A., Rini, P., Taviani, V., and Fletcher, D., "State-to-State Simulation of Nonequilibrium Nitrogen Stagnation-Line Flows: Fluid Dynamics and Vibrational Kinetics," *Journal of Thermophysics and Heat Transfer*, Vol. 22, No. 3, July–Sept. 2008, pp. 390–398.
doi:10.2514/1.34545

[3] Osipov, A. I., and Stupochenko, E. V., "Kinetics of the Thermal Dissociation of Diatomic Molecules I. Small Impurity of Diatomic Molecules in a Monoatomic Inert Gas," *Combustion, Explosion and Shock Waves*, Vol. 10, No. 3, 1974, pp. 303–313.

[4] Billing, G. D., "Rate Constants and Cross Sections for Vibrational Transitions in atom–diatom and diatom–diatom Collisions," *Computer Physics Communications*, Vol. 32, 1984, pp. 45–62.
doi:10.1016/0010-4655(84)90007-9

[5] Billing, G. D., "Rate Constants for Vibrational Transitions in Diatom–Diatom Collisions," *Computer Physics Communications*, Vol. 44, Nos. 1–2, 1987, pp. 121–136.
doi:10.1016/0010-4655(87)90022-1

[6] Billing, G. D., "Vibration–Vibration and Vibration–Translation Energy Transfer, Including Multiquantum Transitions in Atom–Diatom and Diatom–Diatom Collisions," *Topics in Current Physics*, edited by M. Capitelli, Springer–Verlag, Berlin, 1986, pp. 85–111.

[7] Capitelli, M., Gorse, C., and Billing, G. D., "V-V Pumping Up in Nonequilibrium Nitrogen: Effects on the Dissociation Rate," *Chemical Physics*, Vol. 52, No. 3, 1980, pp. 299–304.
doi:10.1016/0301-0104(80)85233-5

[8] Billing, G. D., and Fisher, E. R., "V-V and V-T Rate Coefficients in Diatomic Nitrogen by a Quantum Classical Model," *Chemical Physics*, Vol. 43, No. 3, 1979, pp. 395–401.
doi:10.1016/0301-0104(79)85207-6

[9] Macheret, S. O., and Adamovich, I. V., "Semiclassical Modeling of State-Specific Dissociation Rates in Diatomic Gases," *Journal of Chemical Physics*, Vol. 113, No. 17, Nov. 2000, pp. 7351–7361. doi:10.1063/1.1313386

[10] Adamovich, I. V., and Rich, J. W., "Three-dimensional Nonperturbative Analytic Model of Vibrational Energy Transfer in Atom-Molecule Collisions," *Journal of Chemical Physics*, Vol. 109, No. 18, Nov. 1998, pp. 7711–7724. doi:10.1063/1.477417

[11] Galina, C., Jaffe, R., Schwenke, D. W., and Huo, W., "Dissociation Cross-Sections and Rate Coefficients for Nitrogen from Accurate Theoretical Calculations," AIAA Paper 2008-1209, Jan. 2008.

[12] da Silva, M. L., Guerra, V., and Loureiro, J., "Nonequilibrium Dissociation Processes in Hyperbolic Atmospheric Entries," *Journal of Thermophysics and Heat Transfer*, Vol. 21, No. 2, April–June 2007, pp. 303–310. doi:10.2514/1.26776

[13] Shui, V. H., Appleton, J. P., and Keck, J. C., "Three-Body Recombination and Dissociation of Nitrogen: A Comparison between Theory and Experiment," *Journal of Chemical Physics*, Vol. 53, No. 7, 1970, pp. 2547–2558. doi:10.1063/1.1674368

[14] Armenise, I., Capitelli, M., Colonna, G., Koudriavtsev, N., and Smetanin, V., "Nonequilibrium Vibrational Kinetics During Hypersonic Flow of Solid Bodies in Nitrogen and Its Influence on the Surface Heat Flux," *Plasma Chemistry and Plasma Processing*, Vol. 15, No. 3, 1995, pp. 501–528.

[15] Colonna, G., and Capitelli, M., "The Influence of Atomic and Molecular Metastable States in High- Enthalpy Nozzle Expansion Nitrogen Flows," *Journal of Physics D: Applied Physics*, Vol. 34, Oct. 2001, pp. 1812–1818. doi:10.1088/0022-3727/34/12/308

[16] Colonna, G., Armenise, I., Bruno, D., and Capitelli, M., "Reduction of State-to-State Kinetics to Macro- scopic Models in Hypersonic Flows," *Journal of Thermophysics and Heat Transfer*, Vol. 20, No. 3, July–Sept. 2006, pp. 477–486. doi:10.2514/1.18377

[17] Armenise, I., Esposito, F., and Capitelli, M., "Dissociation-Recombination Models in Hypersonic Boundary Layers," *Chemical Physics*, Vol. 336, 2007, pp. 83–90. doi:10.1016/j.chemphys.2007.05.015

[18] Esposito, F., and Capitelli, M., "QCT Calculations for the Process $N_2(v) + N \rightarrow N_2(v') + N$," *Chemical Physics Letters*, Vol. 418, Nos. 4–6, 2006, pp. 581–585. doi:10.1016/j.cplett.2005.11.036

[19] Armenise, I., Capitelli, M., and Gorse, C., "Nitrogen Nonequilibrium Vibrational Distributions and Non-Arrhenius Dissociation Constants in Hypersonic Boundary Layers," *Journal of Thermophysics and Heat Transfer*, Vol. 12, No. 1, Jan.–March 1998, pp. 45–51. doi:10.2514/2.6300

[20] Armenise, I., and Capitelli, M., "State to State Vibrational Kinetics in the Boundary Layer of an Entering Body in Earth Atmosphere: Particle Distributions and Chemical Kinetics," *Plasma Sources Science and Technology* , Vol. 14, No. 2, May 2005, pp. S9–S17. doi:10.1088/0963-0252/14/2/S02

[21] Capitelli, M., Colonna, G., and Esposito, F., "On the Coupling of Vibrational Relaxation with the Dissociation-Recombination Kinetics: From Dynamics to Aerospace Applications," *Journal of Physical Chemistry A*, Vol. 108, No. 41, 2004, pp. 8930–8934. doi:10.1021/jp048847v

[22] Park, C., *Nonequilibrium Hypersonic Aerothermodynamcis*, Wiley, New York, 1990.

[23] Josyula, E., "Computational Study of Vibrationally Relaxing Gas Past Blunt Body in Hypersonic Flows," *Journal of Thermophysics and Heat Transfer*, Vol. 14, No. 1, Jan. 2000, pp. 18–26. doi:10.2514/2.6505

[24] Giordano, D., Bellucci, V., Colonna, G., Capitelli, M., Armenise, I., and Bruno, C., "Vibrationally Relaxing Flow of N_2 past an Infinite Cylinder," *Journal of Thermophysics and Heat Transfer*, Vol. 11, No. 1, Jan. 1997, pp. 27–35. doi:10.2514/2.6219

[25] Josyula, E., and Bailey, W. F., "vibration–Dissociation Coupling Using Master Equations in Nonequilibrium Hypersonic Blunt-body Flow," *Journal of Thermophysics and Heat Transfer*, Vol. 15, No. 2, April 2001, pp. 157–167. doi:10.2514/2.6604

[26] Josyula, E., and Bailey, W. F., "Vibrational Relaxation and Population Depletion of Nitrogen in Hyper- sonic Flows," AIAA Paper 2002-0200, Jan. 2002.

[27] Josyula, E., Bailey, W. F., and Ruffin, S. M., "Reactive and Nonreactive Vibrational Energy Exchanges in Nonequilibrium Hypersonic Flows," *Physics of Fluids*, Vol. 15, No. 10, Oct. 2003, pp. 3223–3235. doi:10.1063/1.1608013

[28] Landau, L., and Teller, E., "Zur Theorie der Schalldispersion," *Physikalische Zeitschrift der Sowjetunion*, Vol. 10, No. 1, 1936, pp. 34–43.

[29] Millikan, R. C., and White, D. R., "Systematics of Vibrational Relaxation," *Journal of Chemical Physics*, Vol. 39, No. 12, 1963, pp. 3209–3213. doi:10.1063/1.1734182

[30] Josyula, E., and Bailey, W. F., "Vibration–Dissociation Coupling Model for Hypersonic Blunt-Body Flow," *AIAA Journal*, Vol. 41, No. 8, 2003, pp. 1611–1613. doi:10.2514/2.2118

[31] Adamovich, I. V., Macheret, S. O., Rich, J. W., and Treanor, C. E., "Vibrational Relaxation and Dissociation Behind Shock Waves Part 1: Kinetic Rate Models," *AIAA Journal*, Vol. 33, No. 6, June 1995, pp. 1064–1069. doi:10.2514/3.12528

[32] Park, C., "On Convergence of Computation of Chemically Reacting Flows," AIAA Paper 85-0247, Jan. 1985.